Experimental Analysis of the Wake Meandering of a Floating Wind Turbine under Imposed Surge Motion

Experimental Analysis of the Wake Meandering of a Floating Wind Turbine under Imposed Surge Motion

L. Pardo Garcia, B. Conan, S. Aubrun, L. Perret, T. Piquet, C. Raibaudo, B. Schliffke

LHEEA, Centrale Nantes – CNRS UMR 6598, 1 Rue de la Noë, 44300 Nantes, France

E-mail: boris.conan@ec-nantes.fr

Abstract. With the development of floating wind farms, the understanding of the far wake becomes of utmost importance because it cannot only be based on the experience acquired on fixed offshore turbine as the range of motion of the floater due to met-ocean conditions is in the same order of magnitude compared to the energetic turbulent scales of the atmosphere and to the characteristic scales of the wake. The objective of this wind-tunnel experiment is to analyse the behaviour of the wake center of a floating turbine subject to imposed surge motion. The experiment is carried out in the LHEEA wind tunnel where a 1/500 scale wind turbine model is immersed in a realistic offshore atmospheric-boundary layer. The model is actuated in surge by a linear motor able to reproduced idealised second order surge motion of a floating platform (mainly due to the waves) with a realistic amplitude and range of frequencies. Stereoscopic particle image velocimetry measurements are performed at two planes normal to the free-stream at distances of 4.6 and 8.1 diameters downstream of the turbine. Instantaneous velocity fields acquired at 14.1 Hz are individually analysed by convolution to find the location of the wake center. Results show that the wake center spreading is largely influenced by the downstream distance and only slightly affected by the surge motion. However, when analysing the wake position time series by a power spectral density, the signature of the surge motion becomes very clear for both downstream distances. These findings tell that the far wake (at least up to 8.1 diameters downstream) of a floating wind turbine has a "memory" of the motion in its frequency content. When extrapolating to a floating wind farm, this result suggests that a turbine inside a floating wind farm will be immersed in a flow including a significant dynamic signature in the range of its own motion.

1. Introduction

Floating offshore wind is a very promising technology that is expected to experience an important growth in the coming decades, its main advantages are a stronger and more constant wind and a greater social acceptance. With the development of floating wind farms, the understanding of their far wakes becomes of utmost importance because it cannot only rely on the experience acquired on fixed offshore turbine as the motion of the floater due to met-ocean conditions has a similar frequency range $f_{red} = fD/U_{ref} = [0.1, 0.2]$ compared to the energetic turbulent scales of the atmosphere and to the characteristic time scales of the wake. For a floating wind turbine (FWT), an interaction between the floater dynamics, the atmosphere, and the wake is expected and consequences are anticipated on the power curve, the wake meandering, the wake interactions and, finally, on the fatigue of downstream turbines that could potentially challenge current

models.

In the last five years, only a limited number of numerical and experimental studies have been analysing the effect of FWT motions on the far wake with a main interest on pitch and roll motions. Using a rotating wind turbine model at a 1/400 scale, [1, 2, 3] focused their laboratory research on the analysis of the modifications of the wake due to pitch and roll motion in a frequency range of 1.2 Hz - 1.8 Hz with an amplitude of 15°. In their wind tunnel experiment, [5], found that the pitch and roll motion in the range 5° to 20° have a visible signature in the wake of a rotative wind turbine model that vanishes after 7 diameters downstream. Using a porous disk at 1/500 scale in realistic offshore wind conditions, evidence of a signature of a surge motion of an FWT was observed by [7] in the turbulent spectra of the longitudinal component of the velocity up to 8 diameters downstream of the model. In 2021, using a 1/75 scaled rotating wind turbine model and a surge motion actuator, [4] measured the effect of surge motion on the unsteady characteristics of the near wake and found a link with the measured dynamic evolution of the thrust coefficient.

Using numerical simulations, [6] studied the wake interactions of FWTs using several floating technologies (semi-sub, spar and TLP) and underlined increased loads and fatigue and increased motion of the platform in the wake of a first FWT. To now, the literature is still to limited to fully understand all the consequences of having a wind turbine on a floater.

In [7], the signature of surge motion, which are the largest amplitudes for a FWT in a wind/wave aligned scenario, was clearly visible in the far wake, up to 8 diameters downstream of the turbine. The present study aims at contributing to the understanding of FWT wakes dynamics by investigating whether surge motion has an effect on wake meandering by tracking the instantaneous wake center from stereoscopic particle image velocimetry measurements. Two main questions are addressed:

- is there an effect of the surge motion on the wake center statistics?
- is there a signature of the surge motion in the wake meandering?

The experimental set-up, the measurement devices and the wake center detection method are described in Sec. 2. Results for the surge configurations tested are presented in Sec. 3. Section 4 gives a final discussion on the results and their interpretation.

2. Methodology

2.1. Wind tunnel experiment

The experiment is performed in the 2 m x 2 m test section of the atmospheric wind tunnel of the LHEEA lab at Ecole Centrale Nantes. A fence and spires are installed at the start of the test section and perforated plates are placed on the floor, along the 15 m of the test section in order to reproduce the vertical profiles of the mean wind speed, of the turbulence intensity in the three directions and of the turbulent integral length scales representative of an offshore atmospheric boundary-layer at a 1/500 scale. All the details of the inflow conditions can be found in [7]. The good reproduction of inflow conditions, especially the integral turbulent scale is crucial in this study as scales larger than two times the rotor diameter are known to be highly correlated to the wake meandering [8]. In the final configuration, the equivalent full scale integral length scale is 200 m at 150 m.

The wind turbine model represents a 2 MW wind turbine (80 m diameter and 60 m hub height) at 1/500 scale using a D=0.16 m diameter porous disk with a solidity of 45% modelling a C_t of approximately 0.5 [9]. The blockage effect in the test section is below 1%. Porous disks already proved their suitability to analyse the far wake of wind turbines in laboratory

Table 1: Test cases run in the wind tunnel with extrapolation to full scale.

Case number	f [Hz]	f_{red} [-]	$T_{full\ scale}$ [s]
1	0	0	0
2	2	0.084	100
3	3	0.126	67
4	3.75	0.158	53

experiments in a fixed case [9], however, their use in dynamic situations is still to be verified. The surge motion of a floating platform supporting a FWT is the result of the balance between the forces from coming from the wind, waves, current, and the mooring system. It is composed of first order motions (in amplitude) that are induced by the response of the mooring system and of a second order surge motions mainly induced by the sea state. We study here the effect of idealized second order motions into the wind turbine wake in the case where wind and wave are aligned. By means of a linear motor, the model is animated by a sinusoidal surge motion $X(t) = Asin(2\pi ft)$ where the amplitude (A) and the frequency (f) are representative of the most energetic second order surge motion of a 2 MW FWT placed on a barge subject to realistic sea-states. The set-up represents the FLOATGEN FWT installed at the SEM-REV sea test site offshore of Le Croisic (France) with a wave period of $T_p = 11$ s and a significant wave height of $H_s = 4.25$ m [7]. At the scale of the experiment, the amplitude of the motion is set to $A = 10$ mm with a frequency range of f = [0, 2, 3, 3.75] Hz, leading to a reduced frequency range of f_{red} = [0, 0.084, 0.126 and 0.158], with $U_{ref} = 3.8$ m/s the streamwise free-stream velocity at hub height. Using the scaling procedure detailed in [7], the motions reproduced in this experiment corresponds at full scale to an amplitude of ± 5 m in surge and to a period of motion of [0, 100, 67, 53] s. This is in the range of surge periods used in [6]. Test cases are summarized in Tab. 1.

With the limitation that the air-sea dynamic interaction is not reproduced and that the behaviour of the porous disc may be altered while moving, results are expected to give a good idea of the dynamics at play at full scale in the conditions described.

2.2. Measurement set-up

Stereoscopic particle image velocimetry (SPIV) measurements are performed using a Dantec system composed of a 200 mJ laser placed on the ceiling of the test section, pointing downward, and of a set of two HighSense Zyla camera equipped with Nikon 60 mm AF Micro objective lenses in order to measure two vertical span-wise plans (y-z) at $x = 4.6D$ and $x = 8.1D$ downstream from the model where (x, y, z) is an direct frame with x the wind flow direction, z the vertical ascending direction and y the spanwise direction (see on Fig. 1). Cameras are mounted outside of the test section in a symmetrical configuration and Scheimpflug conditions are satisfied using a dedicated camera support. The seeding is generated from a Laskin nozzle using olive oil. For each configuration, around 14 000 image pairs are acquired at a frequency of 14.1 Hz with a time delay between laser pulses of $\Delta t = 350\ \mu$ s.

The SPIV processing is performed using Dantec Dynamic Studio software including a mean image removal, a correlation starting with 128x128 pixels^2 interrogation windows with 2 refinements steps down to 32x32 pixels^2 with an overlapping of 50%, a median filtering, and a stereoscopic reconstruction as a final step. The 3-component velocity field has a final size of 116x105 grid points corresponding to a 641x394 mm^2 in the region $y/D = [-1.99 : 2.01]$ in horizontal and $z/D = [-0.63 : 1.84]$ taking the hub as reference. The final resolution is 5.5 mm in the horizontal direction and 3.5 mm in the vertical direction giving $0.034D$ and $0.023D$,

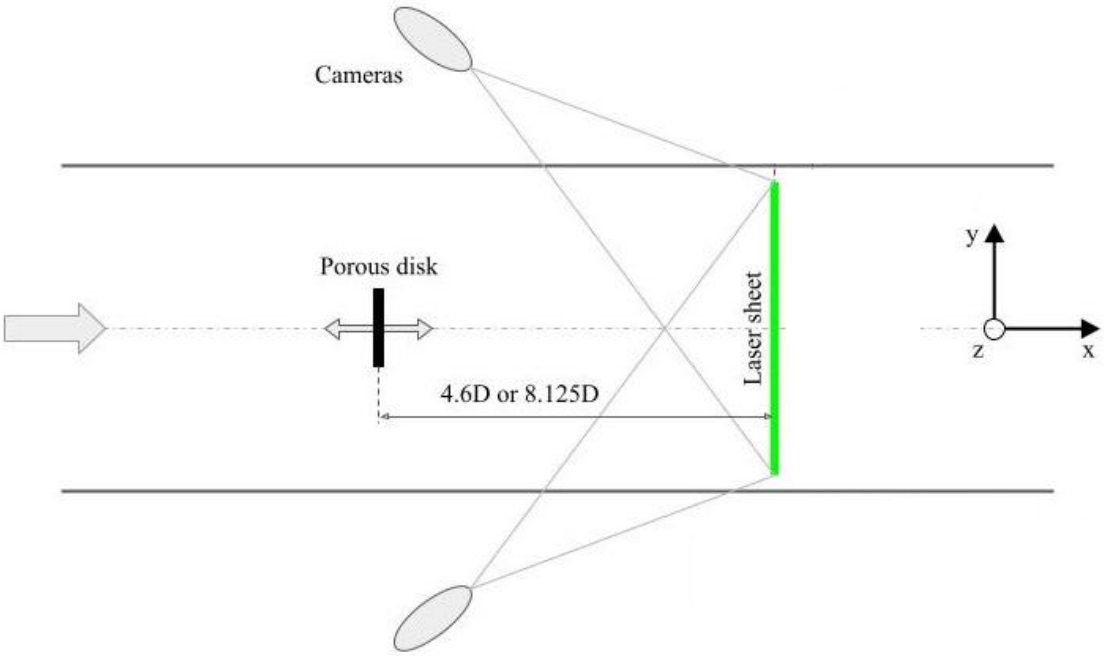

Figure 1: Schematic view of the SPIV set-up underlining the position of the measurement plane (green), the cameras and the model in the test section.

respectively.

2.3. Wake center detection method

In order to study the wake meandering, a tracking method is implemented to detect the wake center from instantaneous SPIV fields. The methodology chosen is a 2D convolution adapted from the algorithm described by [10], who applied it to crossflow velocity fields obtained from numerical simulation. It mainly consists in searching for the maximum of the convolution between the field of instantaneous available power p and a masking function (gaussian kernel) with a diameter D and an amplitude of A_g. This is equivalent to looking for the position of a disk, of diameter D, that has the least available power [10]. The choice of using the available power also magnifies the signal as it is proportional to the cube of the streamwise velocity. Figure 2(a-d) shows an example of the steps followed. To determine the wake center of an instantaneous field (Fig. 2a), the available power, depicted in Fig. 2b, is computed as

$$p = \frac{1}{2} u|u|^2 \tag{1}$$

and then convolved with the masking function (Fig. 2c) defined by

$$f_G(y,z) = A_g \; exp\left(-\left(\frac{y^2}{2\sigma_y^2} + \frac{z^2}{2\sigma_z^2}\right)\right) \tag{2}$$

where $A_g = -1$ and $\sigma_y = \sigma_z = D/4$. The choice of a gaussian masking function and its parametrization is made following the work of [10] to get smooth results. For each SPIV field, the coordinates of the wake center (y_c, z_c) are finally determined at the maximum of the convolution field (Fig. 2d) providing a time series of the position of the wake center. The average wake center ($\overline{y_c}$, $\overline{z_c}$) is used to define $\Delta y = y_c - \overline{y_c}$ and $\Delta z = z_c - \overline{z_c}$.

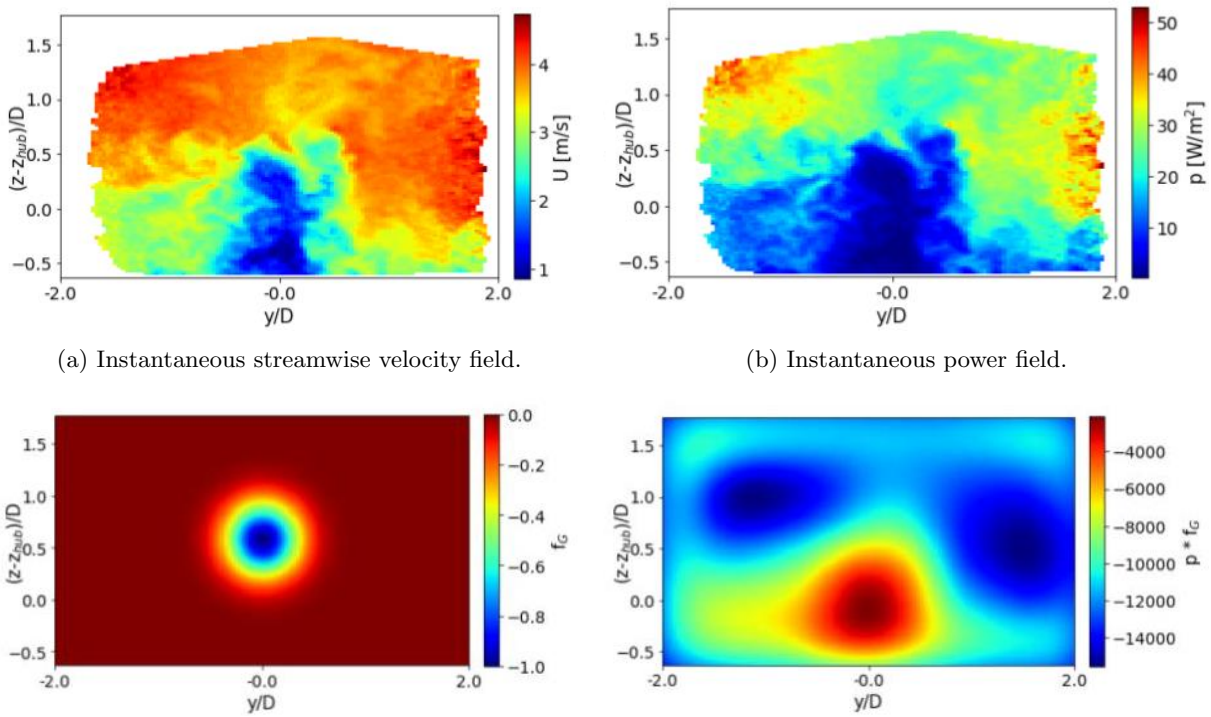

(a) Instantaneous streamwise velocity field.

(b) Instantaneous power field.

(c) Masking function.

(d) Result of the convolution.

Figure 2: Illustrated steps of wake center detection method.

3. Results

3.1. Statistics of the velocity field

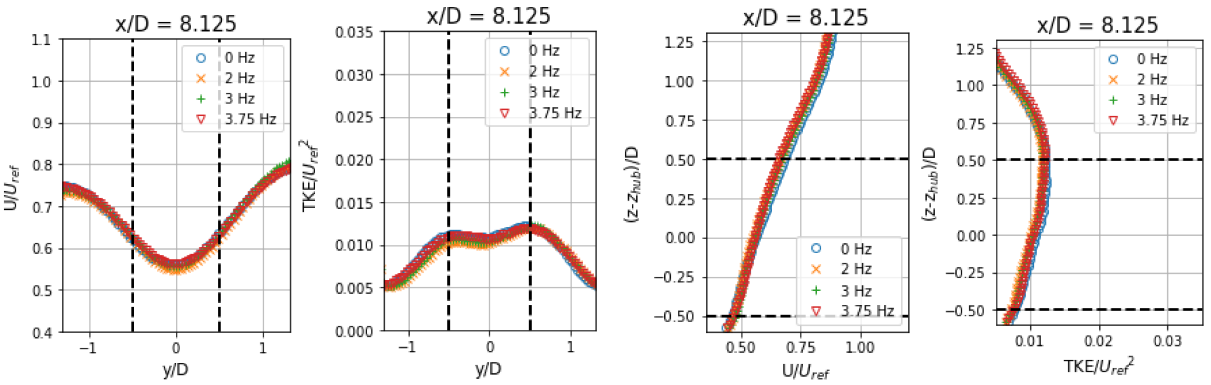

(a) (b) (c) (d)

Figure 3: Comparison of the normalized streamwise velocity and the normalized TKE in an horizontal profile at hub height (a, b) and in a vertical profile at $y/D = 0$ (c, d) for all cases. Vertical black dashed lines show the limit of the rotor area.

The mean velocity components are computed over the 14 000 images acquired and normalized by the reference velocity U_{ref}. The turbulent kinetic energy is computed as $TKE = \frac{1}{2}(\sigma_u^2 + \sigma_v^2 + \sigma_w^2)$, where $(\sigma_u, \sigma_v, \sigma_w)$ are the standard deviation of the velocity in the streamwise, spanwise and vertical directions, respectively.

Profiles of the longitudinal component of the normalized velocity and of the TKE are presented at $x/D = 8.125$ for all surge motions in an horizontal profile at hub height (Fig. 3a,b) and in a vertical profile at $y/D = 0$ (Fig. 3c,d). Results clearly show that, in the far wake, neither the velocity deficit nor the TKE are significantly affected by the surge motion imposed.

3.2. Statistics of the wake center

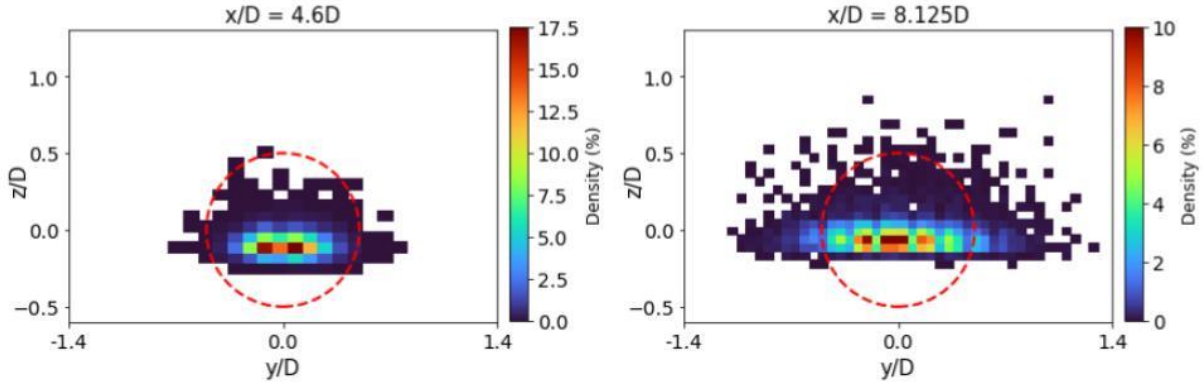

(a) *Case01* at $x/d = 4.6$D (left) and $x/D = 8.1$D (right).

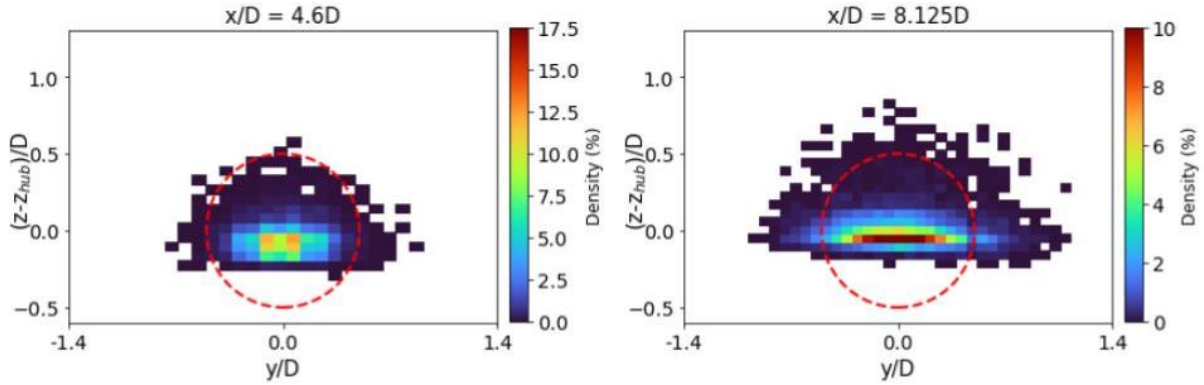

(b) *Case03* at $x/d = 4.6$D (left) and $x/D = 8.1$D (right).

Figure 4: Wake center position density plotted in a 2D histogram.

The wake detection method described in Sec. 2.3 is applied to all test cases at all distances. Figure 4 presents probability distributions of the wake center detected for Case 01 (Fig. 4a) and Case 03 (Fig. 4b) at $x/D = 4.6$ and at $x/D = 8.1$. At $x/D = 4.6$, wake center are mostly detected within the rotor swept area (red-dashed circle in Fig. 4). The span-wise extension of wake center detection shows a symmetric behaviour whereas its vertical extension is unbalanced toward $(z - z_{hub})/D > 0$ due to the presence of the ground, no detection is made below $(z - z_{hub})/D = -0.25$. At $x/D = 8.1$, due to the wake development, results show much more spread, many wake center are detected away from the rotor swept area, often up to $y/D = +/-1$, and sometimes further in the span-wise direction. The vertical extension doesn't follow the same trend as the lowest detections remain above $(z - z_{hub})/D = -0.25$. Qualitatively, the introduction of the surge motion as for case 03 in Fig. 4b, does not have a significant impact on wake center location.

To have a more quantitative evaluation of the distribution and to compare more easily results from all cases, the distribution of Δy in a horizontal line at hub height ($(z - z_{hub})/D = 0$) and

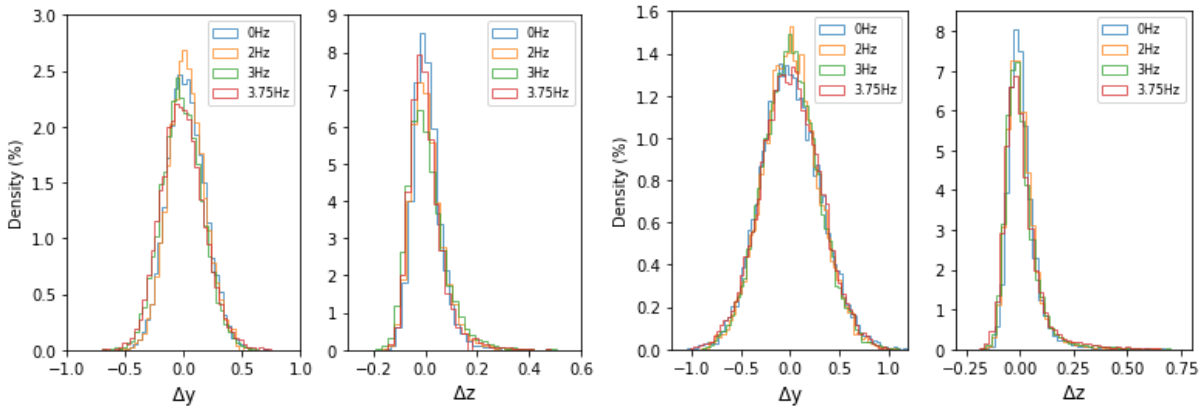

(a) $x/D = 4.6$D. (b) $x/D = 8.1$D.

Figure 5: Probability density distribution of Δy at hub height (left) and Δz at $y/D = 0$ (right) for all cases at both longitudinal positions.

Table 2: Statistics of the wake center position, standard deviation, skewness and normalized kurtosis.

		Standard deviation		Skewness		Kurtosis	
		Δy	Δz	Δy	Δz	Δy	Δz
4.6D	0Hz	0.16	0.06	0.18	1.29	0.12	5.13
	2Hz	0.16	0.07	0.08	1.43	0.22	5.36
	3Hz	0.17	0.08	0.11	1.38	0.16	3.95
	3.75Hz	0.18	0.07	0.21	1.53	0.20	5.23
8.125D	0Hz	0.31	0.08	0.15	2.98	0.09	16.78
	2Hz	0.29	0.08	0.11	2.54	0.08	12.46
	3Hz	0.29	0.09	0.13	2.62	0.03	11.53
	3.75Hz	0.31	0.10	0.00	2.58	-0.05	10.78

the distribution of Δz in a vertical line at the location of the hub ($y/D = 0$) are computed and compared in Fig. 5 for all cases. Global statistics are reported in Tab. 2. In the span-wise direction, the distribution is close to a normal distribution (skewness and kurtosis close to zero) without motion and remains mostly unchanged with the surge motion. The distribution gets closer to a normal distribution with the longitudinal distance. In the vertical direction, due to the presence of the ground surface, the distribution is highly skewed toward positive values, and has a strong positive kurtosis leading to a sharp distribution with a long tail towards $\Delta z > 0$. The skewness and the kurtosis are clearly increasing with the downstream distance meaning that the distribution is getting sharper but is not significantly modified by the surge motion of the model.

3.3. Insight on the unsteady behaviour of the wake center

In the experiments of [7], a significant signature corresponding to the FWT surge motion was observed in the spectrum of the longitudinal component of the velocity at 4.6D downstream of the model. The SPIV performed here is not time resolved, but the acquisition frequency of 14.1 Hz allows to make a spectral analysis up to approximately 7 Hz which is enough to detect whether the imposed motion (3.75 Hz maximum) is visible in the meandering signal.

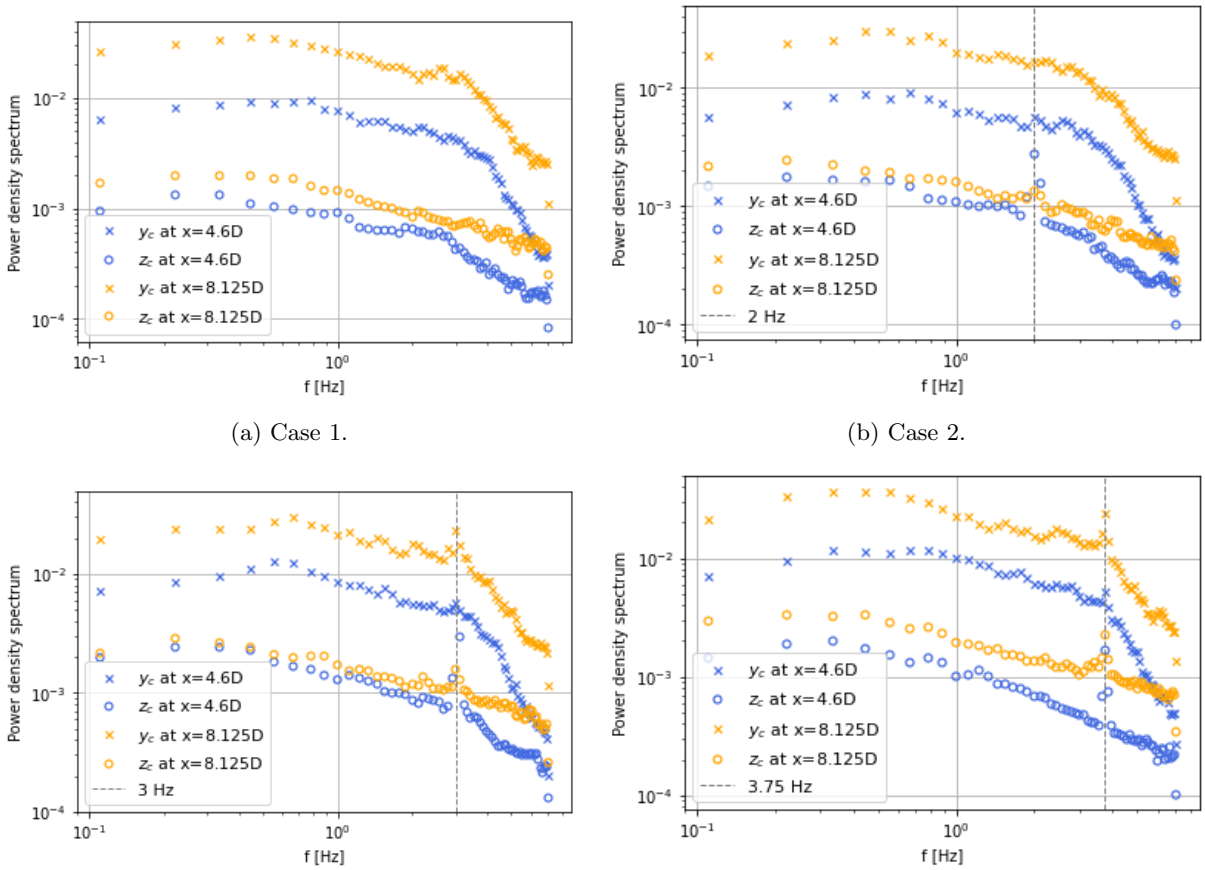

(a) Case 1.

(b) Case 2.

(c) Case 3.

(d) Case 4.

Figure 6: Power spectral density of the vertical (circles) and spanwise (crosses) relative position of the wake center for each motion tested at both downstream positions. The vertical dashed line stands for the imposed surge motion frequency.

For that, the power spectral density of the span-wise and vertical wake position (Δy, Δz) is computed from time series (14 000 points) using the Welch's method with 128 points windowing and 50% overlap. Results, represented in Fig. 6, show a clear and strong spectral signature for Δz at all frequencies tested at $x = 4.6D$. The intensity is relatively decreasing with increasing downstream distance. In the span-wise direction (Δy), the signature of the motion is generally weaker, just emerging from the noise in cases 3 and 4 and only at $x = 4.6D$. Contrary to Δz, the signature of the motion is clearer in Δy for increasing downstream distance.

4. Conclusions

In this work, the analysis of the wake center of a FWT subject to imposed idealized sinusoidal surge motion is studied in a atmospheric boundary-layer wind tunnel at 1/500 scale at two downstream distances $x = 4.6D$ and $x = 8.125D$ using SPIV.

Statistical results show that the wake meandering mainly occurs in the horizontal direction compared to vertical direction and that the spreading of the wake center is highly increased with the downstream distance. However, surge motion, at any frequency in the range tested, has no significant impact. Extrapolating to full scale situations, in terms of mean quantities, surge motion does not significantly modify neither the wake at $x = 8.125D$ nor the meandering. Existing wake meandering models would then be expected to perform equally in evaluating the

wake center of a moving turbine in surge motion as they do for a fixed one.
In the meanwhile, additionally to the spectral signature in the longitudinal velocity component observed by [7] and [4], present results clearly show a signature of the surge motion in the wake meandering time series. This signature is stronger in the vertical direction and remains significant at $x = 8.125D$. These findings tell that the lateral and vertical position of the far wake of a floating wind turbine has a "memory" of the surge motion in its frequency content. The reason for this, somehow unexpected, observation remains unclear but a signature of the surge motion in the vertical and spanwise velocity components was observed by [11] and must have consequences for the wake meandering. Further investigations are needed to elucidate this link.
When extrapolating to a full, this result suggests that a FWT inside a floating wind farm will be immersed in the wake of the previous FWT that includes a significant dynamic signature of the motion of the previous FWT which, in a first approximation, will be in the range of its own motion. This opens potential questions of amplification, phase locking and resonance. Future dynamic wake models may have to take into account the motion of the floater.
These results contribute to the understanding of the wave-structure-wind interaction but are limited to a one-dimensional and monochromatic sinusoidal motion representative of one type of floating technology, the effect of coupled motions with a multi-frequency content, and for several technologies is still to be investigated.

References

[1] Rockel S et al. 2014 Experimental study on influence of pitch motion on the wake of a floating wind turbine model. *Energies* **7.4** 1954-1985
[2] Rockel Stanislav et al 2016 Wake to wake interaction of floating wind turbine models in free pitch motion: An eddy viscosity and mixing length approach. *Renewable Energy* **85** 666-676
[3] Kadum H et al. 2019 Wind turbine wake intermittency dependence on turbulence intensity and pitch motion. *Journal of Renewable and Sustainable Energy* **11.5** 053302
[4] Fontanella A, Bayati I, Mikkelsen R, Belloli M and Zasso A 2021 UNAFLOW: a holistic wind tunnel experiment about the aerodynamic response of floating wind turbines under imposed surge motion *Wind Energy Science* **6** (5), 1169–1190
[5] Fu S, Jin Y, Zheng Y and Chamorro LP 2019 Wake and power fluctuations of a model wind turbine subjected to pitch and roll oscillations. *Applied Energy* **253** 113605
[6] Wise AS, Bachynski EE 2020 Wake meandering effects on floating wind turbines. *Wind Energy* **23**(5) 1266-1285
[7] Schliffke B, Aubrun S and Conan B 2020 Wind tunnel study of a floating wind turbine's wake in an atmospheric boundary layer with imposed characteristic surge motion. *Journal of Physics: Conference Series* **1618**, 062015
[8] Muller YA, Aubrun S and Masson C 2015 Determination of real-time predictors of the wind turbine wake meandering. *Experiments in Fluids*, **56**(3), 1-11
[9] Aubrun S, Loyer S, Hancock PE and Hayden P 2013 Wind turbine wake properties: Comparison between a non-rotating simplified wind turbine model and a rotating model. *Journal of Wind Engineering and Industrial Aerodynamics* **120** 1-8
[10] Coudou N, Moens M, Marichal Y, Van Beeck J, Bricteux L and Chatelain P 2018 Development of wake meandering detection algorithms and their application to large eddy simulations of an isolated wind turbine and a wind farm. *Journal of Physics: Conference Series* **1037** No. 7 072024
[11] Schliffke B 2022 Experimental Characterisation of the Far Wake of a Modelled Floating Wind Turbine as a Function of Incoming Swell. Doctoral dissertation, Ecole Centrale de Nantes *to be published*